Analysis of Turbulence Properties in the Mercury Plasma Environment Using MESSENGER Observations

S. Huang, Q. A. Wang, F. Sahraoui, Z. Yuan, Y. Liu, X. Deng, W. Sun, K. Jiang, S. Xu, X. Yu, et al.

Analysis of Turbulence Properties in the Mercury Plasma Environment Using *MESSENGER* Observations

S. Y. Huang[1], Q. Y. Wang[1], F. Sahraoui[2], Z. G. Yuan[1], Y. J. Liu[1], X. H. Deng[3], W. J. Sun[4], K. Jiang[1], S. B. Xu[1], X. D. Yu[1], Y. Y. Wei[1], and J. Zhang[1]

[1] School of Electronic Information, Wuhan University, Wuhan, People's Republic of China; shiyonghuang@whu.edu.cn
[2] Laboratoire de Physique des Plasmas, CNRS-Ecole Polytechnique-Sorbonne Université-Univ. Paris-Saclay-Observatoire de Paris-Meudon, Palaiseau, France
[3] Institute of Space Science and Technology, Nanchang University, Nanchang, People's Republic of China
[4] Department of Climate and Space Sciences and Engineering, University of Michigan, Ann Arbor, MI, USA
Received 2019 November 26; revised 2020 February 2; accepted 2020 February 4; published 2020 March 16

Abstract

Turbulence is ubiquitous in space and astrophysical plasmas, such as the solar wind, planetary magnetospheres, and the interstellar medium. It plays a key role in converting electric and magnetic energies into kinetic energy of the plasma particles. Here, the properties of MHD and kinetic-scale magnetic fluctuations in the Mercury environment are investigated using data collected by the *MESSENGER* spacecraft from 2011 March 23 to 2015 April 28. It is found that spectral indices at MHD scales vary from $\sim -5/3$ in the near-Planet solar wind (possibly the foreshock) to ~ -1.3 within the magnetosheath close to bow shock. The spectra steepen further in the magnetosheath close to magnetopause, and reach ~ -2.2 within the magnetosphere. Only 15% of events were found to have the Kolmogorov scaling $\sim -5/3$ in the magnetosheath. The high variability of the spectral indices implies that the scaling of turbulent fluctuations in the magnetosheath is not universal, and it emphasizes the role of the bow shock on the turbulence dynamics, at least at the largest scales. Analysis of the magnetic compressibility shows that only $\sim 30\%$ of events with Kolmogorov inertial range in the magnetosheath are dominated by (shear) Alfvénic fluctuations, which contrasts with well-known features of solar wind turbulence. At kinetic scales, the steepest spectra (slopes ~ -2.8) occur in the solar wind, before flattening to ~ -2 near the bow shock, then steepening again to ~ -2.8 in the magnetosheath. The spectral indices at kinetic scales are close to the ones at large scales in the magnetosphere, which may be caused by the presence of heavy ions in the latter. The statistical results are compared with previous observations reported in other planetary plasma environments.

Unified Astronomy Thesaurus concepts: Interplanetary turbulence (829); Plasma astrophysics (1261); Space plasmas (1544); Mercury (planet) (1023); Magnetohydrodynamics (1964); Interplanetary particle acceleration (826)

1. Introduction

Turbulence is ubiquitous in the fluids and plasmas such as atmospheric flows, river rapids, solar wind, planetary magnetospheres, and the interstellar medium etc. (e.g., Tu & Marsch 1995; Bruno & Carbone 2005). In collisionless plasmas, turbulence plays an important role in converting electric and magnetic energies into kinetic energy of thermal (heating) and suprathermal (acceleration) particles (e.g., Bruno & Carbone 2005; Sahraoui et al. 2009, 2010; Huang et al. 2010, 2012; Fu et al. 2017). Therefore, the study of turbulence can help to understand these fundamental physical processes occurring in space plasmas.

In the solar wind, in situ observations from various spacecraft such as *IEEE*, *HELIOS*, *STEREO*, *ACE*, and *WIND*, revealed that the magnetic field spectra have at least three distinct frequency bands separated by two spectral breaks (e.g., Kiyani et al. 2015). At the low frequencies ($\leqslant 10^{-4}$ Hz) is the energy-containing range with a spectral index ~ -1 (Bavassano et al. 1982). In the range $\sim [10^{-4}, 10^{-1}]$ Hz, the spectra steepen to $\sim f^{-5/3}$, which recalls the so-called inertial range of Kolmogorov theory of turbulence (Kolmogorov 1941; Frisch 1995). In MHD turbulence theories, the inertial range is thought to originate from nonlinear interactions between counterpropagating Alfvén wave packets, resulting in the formation of shorter and shorter wavelengths (Iroshnikov 1963; Kraichnan 1965). At higher frequencies from $\sim 10^{-1}$ to $\sim$tens Hz, the spectra steepen further and have an index ~ -2.8, which may be a consequence of both dispersive and dissipation effects, possibly into ion heating (e.g., Goldstein et al. 1995; Leamon et al. 1998; Sahraoui et al. 2010, 2013). At much higher frequencies (~ 100 Hz), a new steepening of the magnetic spectra (to ~ -4) has been reported (e.g., Sahraoui et al. 2009, 2010, 2013; Huang & Sahraoui 2019). In this range, an "ultimate" energy cascade can occur along with dissipation into electron heating (Sahraoui et al. 2009; Schekochihin et al. 2009; Howes et al. 2011).

Turbulence in planetary plasmas has also been investigated in recent years, but with much less details than in the solar wind. Existing studies include the plasma environment of Mars (e.g., Ruhunusiri et al. 2017), Earth (e.g., Sahraoui et al. 2003, 2006; Vörös et al. 2004, 2006; He et al. 2011; Huang et al. 2012, 2014, 2016, 2017a, 2017b, 2017c, 2018; Hadid et al. 2018; Zhu et al. 2019), Saturn (e.g., Hadid et al. 2015; von Papen & Saur 2016), Venus (e.g., Vörös et al. 2008), Jupiter (e.g., Tao et al. 2015), and Mercury (Uritsky et al. 2011). These studies showed similarities and differences between the turbulence in planetary plasmas and that in the solar wind. The similarities include the presence of different spectral power-law bands (with slopes) separated by breaks at ion and electron scales (e.g., Sahraoui et al. 2006; Vörös et al. 2008;

Zimbardo et al. 2010; Huang et al. 2012, 2014, 2017b; Hadid et al. 2015). The spectral indices in the kinetic (or dissipation) range in the Earth's magnetosheath have a median value of −2.8 between ion and electron scales and −5.24 below electron scales (Huang et al. 2014, 2017b), similarly to that reported in the solar wind (Sahraoui et al. 2013). The major differences lie at the MHD scales and concern the dominance of the f^{-1} rather than the Kolmogorov spectrum, which questions the universality of the latter in space plasmas, and the dominance of compressible rather than (shear) Alfvénic fluctuations (Hadid et al. 2015; Huang et al. 2017b).

Mercury is the closest planet in the solar system to the Sun, and it has a magnetic field with the same polarity as Earth's. The magnetic field intensity on its surface is only 1% of the intensity of that on the Earth's surface. Although Mercury's magnetic field is weak, it nevertheless forms a small magnetosphere that interacts with the solar wind (e.g., Winslow et al. 2013). Mercury magnetosheath is demarcated by a bow shock and a magnetopause. Mercury does not have an ionosphere like Earth, but has an exosphere that is mainly composed of heavy particles as shown from *MESSENGER* observations (e.g., Raines et al. 2013). In our study of the Mercury plasma environment, we include the upstream solar wind (and possibly foreshock region), bow shock, magnetosheath, magnetopause, and the magnetosphere. Uritsky et al. (2011) have investigated the kinetic-scale turbulence at Mercury, and found that the turbulence is largely controlled by finite Larmor radius effects. To comprehensively characterize plasma turbulence around Mercury, we carried out a statistical study of the magnetic field fluctuations at MHD and kinetic scales using the in situ observations of *MESSENGER* during the period ranging from 2011 March 23 to 2015 April 28.

2. Data and Results

We used the magnetic field data provided by the MAG instrument (Anderson et al. 2007) and particle data measured by the EPPS instrument (Andrews et al. 2007) on board the *MESSENGER* spacecraft, which are sampled each 0.05 s and 10 s, respectively.

An example of the studied events showing the ion energy spectrum and three components of magnetic field and the corresponding total power spectral density (PSD) is given in Figure 1. The magnetic field is presented in the Mercury Solar Orbital (MSO) coordinate system. One can see that the spacecraft first stayed in the Mercury magnetosphere, then crossed the magnetopause around 06:16 UT and entered into the magnetosheath, and finally passed the bow shock around 07:05 UT and stayed in the solar wind (or foreshock). We observe that the magnetosheath exhibits larger magnetic field fluctuations than the other regions (Figures 1(b)–(c)).

To construct the statistical distribution of the spectral indices of PSDs in the MHD and sub-ion scales, we surveyed all *MESSENGER* data from 2011 March 23 to 2015 April 28. After computing the PSDs, we eliminated the spectra that had large peaks that may be caused by strong wave-like activity (an example is given in Figure 2(b)). Thus, we are left with spectra that have a clear power-law spectrum (Figure 2(a)). For that purpose we used an automated method based on the running slope (Huang & Sahraoui 2019). The method consists in using a sliding window to calculate the spectral slopes with $(2*i+1)$ Δf as the start point and $(5*i+1)\Delta f$ as the end point (where $i = 1, 2...,$ and Δf is 0.0049 Hz). If the difference between the
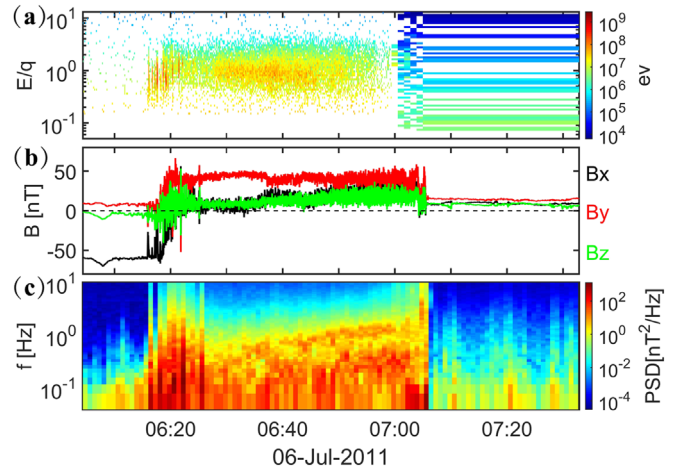

Figure 1. Example of the analyzed data showing the crossing by *MESSENGER* of different regions of the Mercury plasma environments on 2011 July 6: (a) the ion energy spectrum; (b) three components of magnetic field; and (c) the total power spectral densities of the magnetic field. The long horizontal green and blue bars in (a) are not physical, and rather indicate the lack of measurements during this time interval.

spectral slopes of two consecutive frequency bands is less than −0.5 then this is considered as an obvious peak in the magnetic spectrum.

Figure 3 shows the location (and the related density) of all *MESSGENER* observations (Figure 3(a)) and those that showed no significant spectral peaks in the magnetic spectra (Figure 3(b)) in the (X_{mso}, R_{mso}) coordinate system ($R_{mso} = \sqrt{X_{mso}^2 + Y_{mso}^2}$). The bow shock and magnetopause models are also drawn in Figure 3 (Winslow et al. 2013). The bow shock model is described by $\sqrt{(X - X_0)^2 + \rho^2} = p\varepsilon/(1 + \varepsilon \cdot \cos\theta)$ (Slavin et al. 2009), where $X_0 = 0.5$ R_M, $e = 1.04$, $p = 2.75$ R_M, $\rho = \sqrt{Y_{mso}^2 + Z_{mso}^2}$, $\cos\theta = (X - X_0)/R_M$ (R_M is radius of Mercury). The magnetopause model is described by $x(\rho) = -\left(\frac{\gamma^2+1}{4R_{ss}}\right)\rho^2 + R_{ss}$ (Alexeev et al. 2010), where $g = 1$, $R_{ss} = 1.5$ R_M. One can see that *MESSENGER* covers the solar wind and/or foreshock regions, the bow shock, magnetosheath, magnetopause, and magnetosphere of Mercury. The events distribution does not look uniform because of *MESSENGER*'s orbits (Winslow et al. 2013).

Figure 4 shows the spatial distribution of the local proton gyrofrequency estimated using the average of magnetic field each 204.8 s in every grid. One can see that the local ion gyrofrequency is generally smaller than 0.4 Hz in the upstream region, it varies from 0.4 to 0.8 Hz in the magnetosheath, and is about 0.7 Hz in the magnetosphere. This reflects the increase of the magnetic field from the solar wind to the magnetosphere.

To characterize turbulence in various regions of the Mercury plasma environments, we use a power-law fit the PSDs of the magnetic field data in the bands [0.04, 0.4] Hz (MHD range) and [0.8, 4] Hz (kinetic range) to obtain the spectral indices. The PSDs were computed using the fast Fourier transform over time interval of ∼204.8 s, with a sliding window of 10 s. After processing all the data, we constructed the distribution of the spectral indices at MHD scales (Figure 5(a)) and in the kinetic range (Figure 5(b)). One can see that the spectral indices at MHD scales in the upstream region are centered around −1.7, while those in the magnetosphere vary between −2.5 and −2. In the magnetosheath the spectral indices vary from −1.3 near the bow shock to −5/3 toward the flank and subsolar regions,
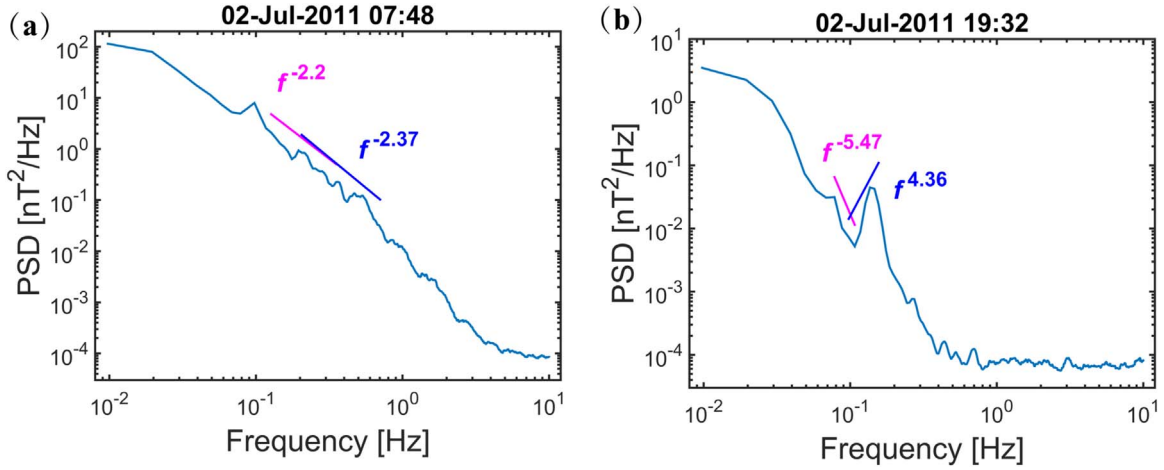
Figure 2. Examples of magnetic field spectrum without a peak (a) and with strong peak (b). The latter were not considered in this study.
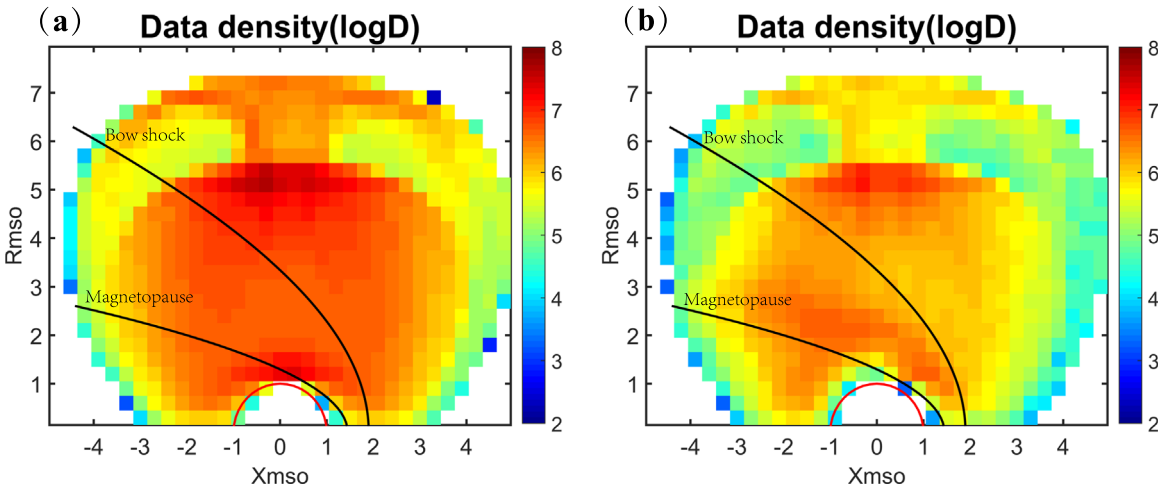

Figure 3. (a) *MESSENGER* orbit coverage map showing data density Dd; (b) *MESSENGER* orbit's data density Dd after eliminating the spectra with a significant wave activities (unit: the number of data points). The black curves indicate the average location of the bow shock (Slavin et al. 2009) and the magnetopause from the models (Alexeev et al. 2010), and the red curve presents Mercury. The size of each pixel is 0.3 R_M.
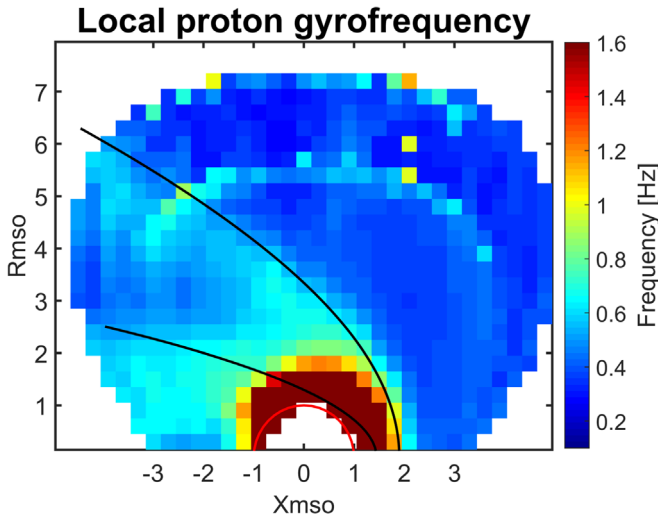

Figure 4. Mean local proton gyrofrequency in the X_{mso} vs. R_{mso} plane.

which agrees with the results reported from the Earth's magnetosheath (Huang et al. 2017b). Only 15% of the events have Kolmogorov-like inertial range (with spectral indices

from −1.77 to −1.55). Figure 5(b) (kinetic range) shows a clear transition in the spectral slopes between the solar wind and the inner magnetosheath: they vary from ∼−2.8 in the solar wind, then flatten to −2 near the shock (or foreshock) region, before steepening to −2.7 in the inner magnetosheath. In the magnetosphere, the spectra are the steepest at MHD scales (slopes ∼−2.3), while at kinetic scales the spectra are rather shallower than in the other regions.

To determine the change trend of the spectral indices from MHD range to kinetic ranges, we selected four subregions in the Mercury plasma environment (marked in the Figure 5(a)) to plot the averaged PSDs in Figure 6. On can observe that the spectra show a break around the proton gyrofrequency (Figures 6(a)–(c)), but not the spectrum in the magnetosphere (Figure 6(d)). In the upstream region, the PSD at MHD scales follows Kolmogorov's scaling, and steepens to ∼−2.53 at kinetic scale (Figure 6(a)), in agreement with previous observations in solar wind turbulence (e.g., Sahraoui et al. 2009, 2010; Kiyani et al. 2015; Huang & Sahraoui 2019). The spectral index in the magnetosheath at MHD range is flatter than −5/3 of the Kolmogorov's closer to the bow shock (Figure 6(b)), and approaches the Kolmogorov's index closer to magnetopause (Figure 6(c)). In the magnetosphere (Figure 6(d)), the spectrum at MHD scales is the steepest (slope
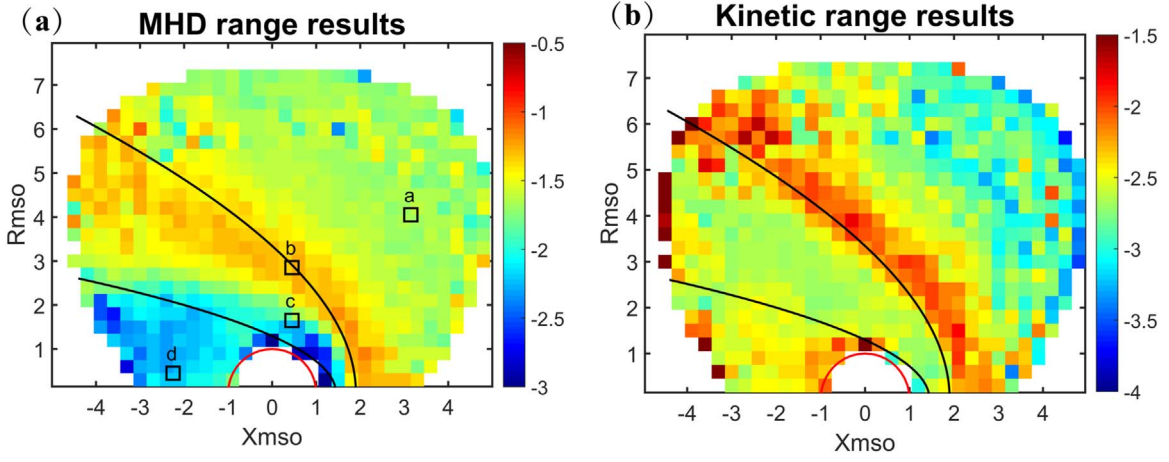
Figure 5. Spatial distribution of the spectral indices at MHD scales (a) and in the sub-ion (kinetic) range (b) given in the (X_{mso}–R_{mso}) plane.
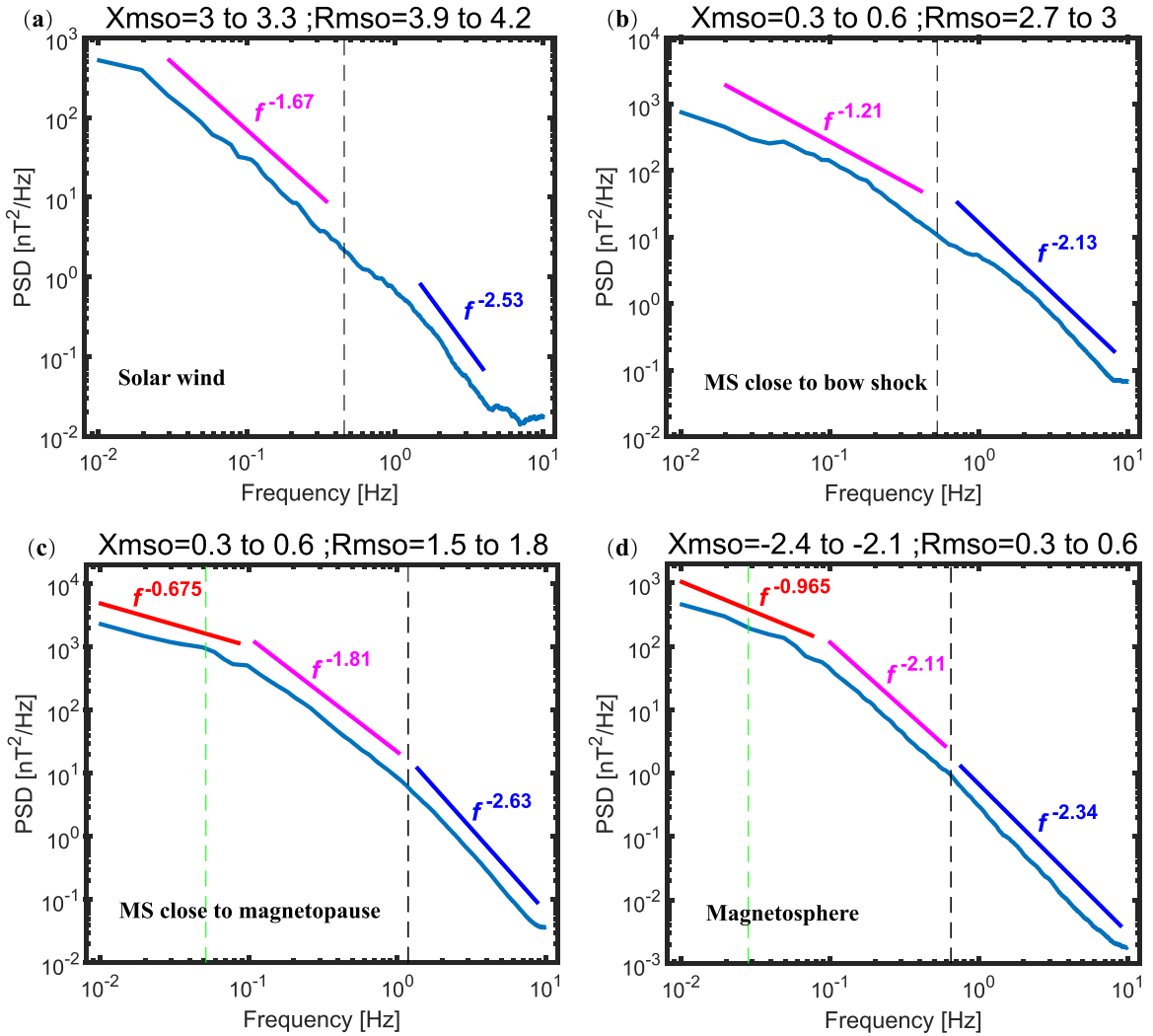

Figure 6. Spectral power densities in four different subregions of the Mercury plasma environment indicated by "abcd" with black squares in Figure 4(a). Local proton gyrofrequencies are shown by the black dashed lines. Na+ gyrofrequencies are marked by green dashed lines in (c)–(d). Magnetosheath is abbreviated by "MS."

~-2.13) compared with other three regions and is very close to that in the kinetic range.

To investigate the nature of turbulent fluctuations that have Kolmogorov-like spectrum (slopes ~-1.77 to -1.55) in the Mercury's magnetosheath, we calculated the magnetic

compressibility given by the ratio between the parallel (with respect to the background field B_0) PSDs and the total magnetic field fluctuation, i.e., $C_{\parallel}(f) = |\delta\mathrm{B}_{\parallel}(f)|^2/(|\delta\mathrm{B}_{\parallel}(f)|^2 + |\delta\mathrm{B}_{\perp}(f)|^2)$. Indeed, shear Alfvénic turbulence is characterized by small magnetic compressibility at MHD scales (typically $C_{\parallel} < 1/3$),
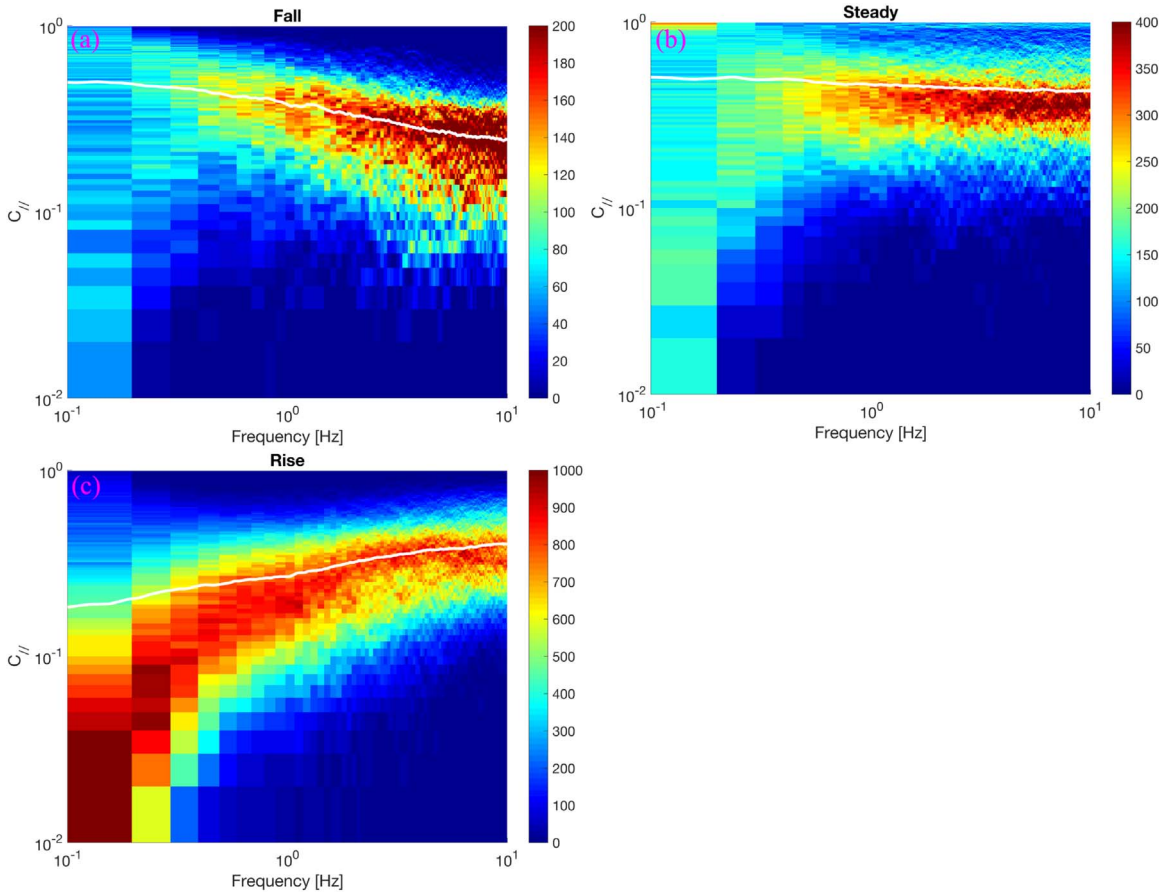
Figure 7. Magnetic compressibility $C_\parallel$ for the statistical events in the magnetosheath with the MHD range spectral indices from -1.77 to -1.55 (i.e., centered at Kolmogorov's index -1.66). Three distinct groups were found: (a) falling off and (b) steady, both characteristic of compressible magnetosonic-like turbulence; and (c) the rising characteristic of shear Alfvén wave turbulence. The white curves are median values. The colors represent the number of events in each bin.

while compressible magnetosonic (fast or slow-like modes) have higher $C_\parallel$ (e.g., Gary et al. 2012; Podesta & Tenbarge 2012; Sahraoui et al. 2012; Salem et al. 2012; Kiyani et al. 2013; Huang et al. 2017b). Figure 7 shows the statistical results on the magnetic compressibility obtained for all the events that have a Kolmogorov-like spectrum in the magnetosheath. Three distinct profiles were evidenced: a falling off and steady profiles with $C_\parallel > 1/3$ (Figures 7(a)–(b)), reflecting the dominance of compressible magnetosonic-like modes, and a rising profile with $C_\parallel < 1/3$, characteristic of the shear Alfvén mode. The latter represented only ~30% of the total number of events, in agreement with similar observations in the Earth's magnetosheath (Huang et al. 2017b). Note that a power isotropy (i.e., $C_\parallel \sim 1/3$) is reached at frequencies $f \sim 10$ Hz in particular for rising and falling-off profiles, which can be physical (Sahraoui et al. 2012) or due to reaching the noise floor of the instrument (assuming that the three triaxial MAG sensors have the same noise floor).

3. Discussions

Unlike the solar wind turbulence, the Kolmogorov spectrum is not ubiquitous in the Mercury plasma environment. In particular, the spectral indices at MHD scales deviate from the Kolmogorov's index $-5/3$ in the vicinity of the bow shock. The deviation in the upstream region may be caused by the presence of the reflected particles from the bow shock and the associated plasma instabilities (e.g., Lucek et al. 2005).

The deviation in the downstream region may indicate the role of the bow shock in "resetting" the turbulence dynamics, which results in shallower spectra close to f^{-1}, as suggested in Hadid et al. (2015) and Huang et al. (2017b). However, the Kolmogrov spectrum is recovered in the inner magnetosheath closer to the flanks of the magnetopause, possibly because turbulence has enough time to reach a fully developed state as it evolves from the bow shock to the magnetopause. Another possible explanation is the local (i.e., at the flanks of the magnetopause) generation by large-scale instabilities such as the Kelvin–Helmoltz (Hwang et al. 2011). These results are similar to the observations in the Earth's magnetosheath (Huang et al. 2017b), Saturn's magnetosheath (Hadid et al. 2015) and Mars magnetosheath (Ruhunusiri et al. 2017). Numerical simulations should help answering this question about the local versus self-consistent generation of fully developed turbulence at the magnetopause flanks.

In the kinetic range, the spectral indices in the Mercury upstream region are similar to those reported in the solar wind turbulence, ~$[-3.3, -2.5]$. However, the spectra become shallower (slopes ~-2) near the bow shock, which may due to the presence of ion instabilities caused by the reflected particles (e.g., Eastwood et al. 2005). This feature is also observed in the Martian environment (Ruhunusiri et al. 2017).

The spectral indices at the frequency range from 0.04 to 4 Hz in the magnetosphere show peculiar features not seen in the outer regions, e.g., slopes ~-2.34 at frequencies larger than

the local proton gyrofrequency, and ~ -2.11 just below the local proton gyrofrequency. Considering that the dominant species in the Mercury magnetosphere are heavy ions coming from its exosphere, such as natrium (Na) and calcium (Ca) (Raines et al. 2013), the gyrofrequency of such heavy ions is about 0.01–0.017 Hz. This value corresponds roughly to the spectral break observed in Figure 6(d) (Na^+ gyrofrequency is displayed by vertical green dashed line). Based on these arguments, the frequency range from 0.04 Hz to 4 Hz would be rather considered as a kinetic (dissipation) range, which then would explain the steep spectra (slopes ~ -2.2) observed in that range. To our knowledge this type of turbulence has not been studied before, thus it requires further exploration, in particular in the case where protons constitute a nonnegligible component of the ions.

4. Conclusions

In the present study, we investigated the properties of turbulence in Mercury plasma environments using a large sample of *MESSENGER* data. We focused on the spectral indices at MHD and kinetic scales, and constructed their spatial distribution in different regions of the Mercury environment. It is found that the MHD range spectral indices increase when moving from the solar wind ($\sim -5/3$) to the bow shock (~ -1.3), then decrease from the nearby of the bow shock to the magnetopause and magnetosphere (~ -2.2). The kinetic range spectral indices have the same trend when moving from the solar wind to the magnetopause, then increase from the magnetopause to the magnetosphere. The statistical results imply that there is no universal Kolmogorov inertial range in the magnetosheath plasma, and that the interaction with the bow shock re-sets the turbulence dynamics pre-existing in the solar wind. However, a fully developed turbulence state is recovered away from the bow shock toward the flanks of the magnetopause where the Kolmogorov spectrum is observed. In addition, in the magnetosheath only $\sim 30\%$ of the Kolmogorov-like events were found to be dominated by Alfvénic fluctuations, which is very different from the solar wind turbulence. This suggests that the Kolmogorov inertial range can be caused by the compressible magnetosonic-like modes (i.e., fast and slow magnetosonic modes). The increase of the spectral indices at kinetic scales in the upstream foreshock might be caused by the reflected particles from the bow shock and associated plasma instabilities. In the magnetosphere, a new turbulence regime based on a plasma dominated by heavy ions might explain the observed steep spectra (slopes ~ -2.2) at frequencies above the local proton gyrofrequency, which is generally referred to as the MHD range in proton-electron plasma. A new multi-ion species model might be necessary to develop if one wants to better interpret these observations.

References

Alexeev, I. I., Elena, S. Belenkaya, Slavin, James A., et al. 2010, Icar, 209, 23
Anderson, B. J., Acuña, M. H., Lohr, D. A., et al. 2007, SSRv, 131, 417
Andrews, G. B., Zurbuchen, T. H., Mauk, B. H., et al. 2007, SSRv, 131, 523
Bavassano, B., Dobrowolny, M., Mariani, F., & Ness, N. F. 1982, JGR, 87, 3617
Bruno, R., & Carbone, V. 2005, LRSP, 2, 4
Eastwood, J. P., Lucek, E. A., Mazelle, C., et al. 2005, SSRv, 118, 41
Frisch, U. 1995, Turbulence (Cambridge: Cambridge Univ. Press)
Fu, H. S., Vaivads, A., Khotyaintsev, Y. V., et al. 2017, GeoRL, 44, 37
Gary, S. P., Chang, O., & Wang, J. 2012, ApJ, 755, 142
Goldstein, M. L., Roberts, D. A., & Matthaeus, W. H. 1995, ARA&A, 33, 283
Hadid, L., Sahraoui, F., Kiyani, K. H., et al. 2015, ApJL, 813, L29
Hadid, L. Z., Sahraoui, F., Galtier, S., & Huang, S. Y. 2018, PhRvL, 120, 055102
He, J. S., Marsch, E., Tu, C. Y., et al. 2011, JGR, 116, A06207
Howes, G. G., TenBarge, J. M., & Dorland, W. 2011, PhPl, 18, 102305
Huang, S. Y., Du, J. W., Sahraoui, F., et al. 2017a, JGRA, 122, 8577
Huang, S. Y., Hadid, L. Z., Sahraoui, F., et al. 2017b, ApJL, 836, L10
Huang, S. Y., & Sahraoui, F. 2019, ApJ, 876, 138
Huang, S. Y., Sahraoui, F., Deng, X. H., et al. 2014, ApJL, 789, L28
Huang, S. Y., Sahraoui, F., Retino, A., et al. 2016, GeoRL, 43, 7850
Huang, S. Y., Sahraoui, F., Yuan, Z. G., et al. 2017c, ApJL, 836, L27
Huang, S. Y., Sahraoui, F., Yuan, Z. G., et al. 2018, ApJ, 861, 29
Huang, S. Y., Zhou, M., Sahraoui, F., et al. 2010, JGR, 115, A12211
Huang, S. Y., Zhou, M., Sahraoui, F., et al. 2012, GeoRL, 39, L11104
Hwang, K.-J., Kuznetsova, M. M., Sahraoui, F., et al. 2011, JGR, 116, A08210
Iroshnikov, P. S. 1963, AZh, 40, 742
Kiyani, K. H., Chapman, C., Sahraoui, F., et al. 2013, ApJ, 763, 10
Kiyani, K. H., Osman, K. T., & Chapman, S. C. 2015, RSPTA, 373, 20140155
Kolmogorov 1941, DoSSR, 30, 301
Kraichnan, R. H. 1965, PhFl, 8, 1385
Leamon, R. J., Smith, C. W., Ness, N. F., et al. 1998, JGR, 103, 4775
Lucek, E. A., Constantinescu, D., Goldstein, M. L., et al. 2005, SSRv, 118, 95
Podesta, J. J., & Tenbarge, J. M. 2012, JGRA, 117, A10106
Raines, J. M., Gershman, D. J., Zurbuchen, T. H., et al. 2013, JGRA, 118, 1604
Ruhunusiri, S., Halekas, J. S., Espley, J. R., et al. 2017, JGRA, 122, 656
Sahraoui, F., Belmont, G., & Goldstein, M. L. 2012, ApJ, 748, 100
Sahraoui, F., Belmont, G., Rezeau, L., et al. 2006, PhRvL, 96, 075002
Sahraoui, F., Goldstein, M. L., Belmont, G., & Rezeau, C. P. 2010, PhRvL, 105, 131101
Sahraoui, F., Goldstein, M. L., Robert, P., & Khotyaintsev, Y. V. 2009, PhRvL, 102, 231102
Sahraoui, F., Huang, S. Y., Belmont, G., et al. 2013, ApJ, 777, 15
Sahraoui, F., Pinçon, J. L., Belmont, G., et al. 2003, JGRA, 108, 1335
Salem, C. S., Howes, G. G., Sundkvist, et al. 2012, ApJL, 745, L9
Schekochihin, A. A., Cowley, S. C., Dorland, W., et al. 2009, ApJS, 182, 310
Slavin, J. A., Anderson, B. J., Zurbuchen, T. H., et al. 2009, GeoRL, 36, L02101
Tao, C., Sahraoui, F., Fontaine, D., et al. 2015, JGRA, 120, 2477
Tu, C. Y., & Marsch, E. 1995, SSRv, 73, 1
Uritsky, V. M., Slavin, J. A., Khazanov, G. V., et al. 2011, JGR, 116, A09236
von Papen, M., & Saur, J. 2016, JGRA, 121, 4119
Vörös, Z., Baumjohann, W., Nakamura, R., et al. 2004, JGRA, 109, 11215
Vörös, Z., Baumjohann, W., Nakamura, R., Volwerk, M., & Runov, A, A. 2006, SSRv, 122, 301
Vörös, Z., Nakamura, R., Sergeev, V., et al. 2008, JGRA, 113, A07S29
Winslow, R. M., Anderson, B. J., Johnson, C. L., et al. 2013, JGRA, 118, 2213
Zhu, X., He, J., Verscharen, D., & Zhao, J. 2019, ApJ, 878, 48
Zimbardo, G., Greco, A., Sorriso-Valvo, L., et al. 2010, SSRv, 156, 89